Magnetic Resonance Imaging 33 (2015) 701–708

Contents lists available at ScienceDirect

Magnetic Resonance Imaging

journal homepage: www.mrijournal.com

Original contributions

Improvement of renal diffusion-weighted magnetic resonance imaging with readout-segmented echo-planar imaging at 3 T

Iris Friedli [a,*], Lindsey A. Crowe [a], Magalie Viallon [a], David A. Porter [b], Pierre-Yves Martin [c], Sophie de Seigneux [c], Jean-Paul Vallée [a,*]

[a] Division of Radiology, Department of Radiology and Medical Informatics, Geneva University Hospitals and Faculty of Medicine of the University of Geneva, Switzerland
[b] Siemens AG, Healthcare Sector, Erlangen, Germany
[c] Division of Nephrology, Geneva University Hospitals and Faculty of Medicine of the University of Geneva, Switzerland

ARTICLE INFO

Article history:
Received 1 October 2014
Accepted 20 February 2015

Keywords:
Readout-segmented EPI
RESOLVE
Renal
Diffusion-weighted MRI
Artifacts

ABSTRACT

Purpose: To assess the feasibility of a respiratory-gated implementation of readout-segmented SE-EPI (RESOLVE) for renal diffusion-weighted imaging (DWI) by comparison with single-shot SE-EPI (ss-EPI) in a phantom, healthy volunteers and chronic kidney disease (CKD) patients.

Materials and Methods: A fluid-filled phantom, 20 healthy volunteers and 10 CKD patients were scanned with the same parameters and coils on a 3 T MR system with 3 DW sequences (b-values = 0, 300, 500, 900 s/mm^2): a standard ss-EPI (Reference EPI), a ss-EPI with higher resolution, bandwidth and acceleration factor (HR-EPI) and RESOLVE with the same spatial resolution as HR-EPI but a segmentation of the readout into 5 shots. Geometric distortions, image blurring using a 'Canny' edge detection based measure, cortico-medullary differentiation measured on b_0 images and ADC quantification were compared between the 3 sequences using one-way analysis of variance (ANOVA) with post-hoc Bonferroni ($p < 0.05$ was taken as statistically significant).

Results: RESOLVE reduced significantly geometric distortions and blurring and improved, in the volunteers and patients, the sharpness score by 56% on average in comparison to ss-EPI ($p = 0.02$). In healthy volunteers, the cortico-medullary differentiation with RESOLVE was also possible on a wider range of b-values ($p < 0.02$) with ADC values (in 10^{-6} mm^2/s) of 1994 ± 246 in the cortex and 1762 ± 238 in the medulla ($p < 0.001$). In CKD patients, ADC values (in 10^{-6} mm^2/s) from the RESOLVE sequence were not different between the cortex (1755 ± 145) and the medulla (1799 ± 163, $p = 0.49$).

Conclusion: Despite a longer scan time, RESOLVE enhanced significantly the quality of renal diffusion-weighted images by improving the difference in SI and ADC between the renal cortex and medulla in healthy volunteers. In CKD patients, RESOLVE showed a disappearance of this cortico-medullary ADC difference. These improvements justify further clinical studies.

1. Introduction

Diffusion-Weighted MR Imaging (DWI) has shown promising results to differentiate pathological from healthy tissues in renal tumors [1], transplant rejection [2], pyelonephritis [3], ureteral stone obstruction [4] and renal artery stenosis [5]. DWI techniques used in the abdomen rely on single-shot diffusion-weighted echo-planar imaging (ss-EPI) which is sensitive to image artifacts [6]. The trade-off between resolution and signal-to-noise ratio for the large FOV used in the abdomen imposes an increased matrix size and therefore a longer EPI readout time. The sequence becomes more sensitive to in-plane geometric distortions caused by the off-resonance water protons in areas where a significant difference in susceptibility exists. In renal DW applications, severe distortions are present at the bowel (filled with air) and tissue interface.

One solution to improve the distortions in diffusion MRI is to use a 'Readout Segmentation Of Long Variable Echo-trains' (RESOLVE) MR sequence in combination with parallel imaging technique, such as GRAPPA, GeneRalized Autocalibrating Partially Parallel Acquisitions. The RESOLVE strategy is based on a segmentation of k-space into several shots along the readout direction in order to shorten the echo spacing. RESOLVE combined with parallel imaging was previously introduced by Porter et al. for acquiring high-resolution DW images with low susceptibility based image distortion and T_2^* blurring in the brain [7]. This strategy has been validated in non-triggered applications, such as in head and breast imaging to

* Corresponding authors at: Department of Radiology, Geneva University Hospitals, Rue Gabrielle-Perret-Gentil 4, 1211 Geneva, Switzerland. Tel.: +41 22 372 5228; fax: +41 22 37 27072.
E-mail addresses: Iris.Friedli@unige.ch (I. Friedli), Jean-Paul.Vallee@hcuge.ch (J-P. Vallée).

http://dx.doi.org/10.1016/j.mri.2015.02.023
0730-725X/

reduce sensitivity to susceptibility artifacts [8–10]. RESOLVE outperformed ss-EPI for analysis of the pediatric brain in regions prone to geometric distortions, such as the orbit, the skull base, and the posterior fossa [11]. By comparison with a conventional ss-EPI sequence, RESOLVE has improved the lesion-to-background contrast and the categorization between benign and malignant breast lesions [12]. For these reasons, we hypothesized that RESOLVE could improve the robustness against artifacts that are a consequence of the long k-space sampling in renal DWI. We proposed in this study an implementation of a respiratory-gated RESOLVE protocol for kidney DWI as well as a comparison of image quality with a different implementation of ss-EPI in a phantom, healthy volunteers and chronic kidney disease (CKD) patients.

2. Materials and methods

2.1. Subjects

Twenty healthy volunteers, comprising 11 females and 9 males, with a mean age of 28.8 ± 4.7 years (range, 23–39 years) and ten patients, comprising 4 females and 6 males, with a mean age of 55 ± 16 (ranges 26–78 years), were recruited after informed consent. Healthy volunteers enrolled in this study had no known kidney disease. All patients were chronic kidney disease (CKD) patients, comprising 1 native kidney and 9 allograft patients. The patients' characteristics are summarized in Table 1. The study protocol was approved by the local ethics committee (reference no. CER-1-160).

2.2. Phantom study

A standard cylindrical phantom filled with deionized water doped with phenol, sodium chloride and copper sulphate (Picker International, model No 374486, diameter 18.7 cm) was used in the experimental comparison.

2.3. MRI technique

The phantom, healthy volunteers and patients were scanned with the same imaging parameters and coils on a MAGNETOM Trio 'Tim system' clinical 3 T MR (Siemens AG, Erlangen, Germany) with a 200 T/m/s slew rate capability. In all cases, the images were acquired using the 6 element phased–array abdominal coil and the spine coil integrated into the scanner table. The protocol included two navigator-triggered ss-EPI MR scans using PACE (prospective acquisition correction technique) and the RESOLVE diffusion-weighted SE-EPI (Spin Echo based EPI) acquisition synchronized to the patient respiration using a respiratory belt. The use of a navigator to trigger ss-EPI DWI was chosen as it improves image quality and enables a more precise ADC quantification in the liver, compared to free breathing [13]. The first navigator-triggered ss-EPI was implemented with the parameters recommended for clinical practice [14,15] hereafter called 'reference EPI', and the second MR sequence was optimized for a higher resolution with an increased matrix, bandwidth and acceleration factor, called hereafter 'HR-EPI'. In all the 3 diffusion MR sequences (ss-EPI and RESOLVE), a bipolar diffusion scheme was used instead of a monopolar approach to decrease eddy current effects resulting from the diffusion-encoding gradient pulses [16]. The diffusion-encoding gradients were applied in 3 orthogonal directions with 4 b-values (0, 300, 500 and 900 seconds/mm^2). All DWI sequences were performed using the parallel imaging GRAPPA technique (acceleration factor = 2 for reference EPI and 3 for HR-EPI and RESOLVE) with the acquisition of 6 coronal–oblique slices of 5 mm each covering the kidney. Shim settings and image positioning were strictly identical for all DW imaging sequences. The different DW sequence parameters used for the study for both phantom and in vivo (healthy subjects and patients) scans are summarized in Table 2. A gradient echo (GRE) sequence with parameters TR/TE = 711/1.09 ms, flip angle 35°, FOV 379 × 328 mm, matrix size 192 × 133 mm, slice thickness 5 mm, acceleration factor 2, bandwidth 930 Hz/pixel was also performed to give reference anatomic images for the comparison of edge geometric distortions and region of interest (ROI) positioning in volunteers and patients.

Table 1
Patients' characteristics.

Study population	9 allograft patients + 1 native kidney
Gender of participant	4 females and 6 males
Age	55 ± 16 (range, 26–78 years)
eGFR ml/min/1.73m^2	49 ± 16 (range, 10–66)

2.4. Analysis of phantom studies

2.4.1. Geometric distortions

The level of geometric distortions was quantified with the use of the phantom to benefit from stable and reproducible conditions without the disadvantages of physiological noise or motion that could occur during the MR acquisition in a volunteer. For quantitative evaluation of geometric distortions, the DW images were resampled to have an identical matrix to the GRE images. Then, the diffusion images and GRE images used as reference were fused with the OsiriX fusion tool plugin (OsiriX Open source http://www.osirix-viewer.com/). Geometric distortions were measured as the maximum distance in the phase-encoding direction between the phantom edges of the diffusion image and of the GRE image on the fused image.

2.5. Analysis of in vivo images

2.5.1. Geometric distortions

Geometric distortions due to susceptibility artifacts were qualitatively evaluated on the b_0 images. The contours of the kidney were drawn manually on the GRE images of healthy volunteers and patients and copied to all DW images with the OsiriX ROI tool.

2.5.2. Blurring

The T_2^* blurring effect due to the peak broadening of the point-spread function (PSF) [17] was evaluated on the RESOLVE and HR-EPI images only, as they had comparable resolution. Reference EPI was not included in this evaluation, as the lower resolution would not give comparable results. To compare the image degradation, an algorithm based on a 'Canny' edge detector [18] was developed with MATLAB® (R2012b, MathWorks, USA) to detect the renal edges and quantitatively evaluate the sharpness of the kidney.

Table 2
DWI MR parameters.

	Reference EPI	HR-EPI	RESOLVE
FOV [mm]	400 × 400	400 × 336	397 × 342
Matrix size	128 × 128	200 × 168	196 × 167
TE [ms]	71	68.4	68
TR minimum/slice [ms]	120	130	140
Echo spacing [ms]	0.73	0.69	0.32
Section thickness [mm]	5	5	5
Intersection gap [mm]	1	1	1
GRAPPA factor	2	3	3
Bandwidth [Hz/pixel]	1500	2272	981
Number of readout segments	1	1	5
Number of signal acquisition	1	1	1
Respiratory gating	PACE	PACE	Belt
b-values [s/mm^2]	0, 300, 500, 900	0, 300, 500, 900	0, 300, 500, 900
Mean scan time	1'7"	1'11"	5'63"

After image normalization, the same ROI was manually defined around the kidney on the images of both sequences. The selected region encompassed the entire kidney as closely as possible to avoid confounding pixels from other organs. The image was smoothened by a Gaussian filter ($\mu = 0.1$, $\sigma = 1$) to reduce the noise, and then the gradient of the image was computed. After getting gradient images, non-maximum suppression was done to find edges in the gray-scale image by looking for local maxima in the direction of gradient with pixels checked for a local maximum in their neighborhood. After the full scan of the image to remove any unwanted pixels that were not classified as a real edge, a hysteresis thresholding discarded non-edge pixels based on their connectivity. Two thresholds were used to perform the hysteresis thresholding in order to track the remaining pixels that had not already been suppressed. The sensitivity threshold was set empirically to 0.4 for the upper threshold (UT) and to 0.16 for the lower threshold (LT) (automatically calculated as 40% of the UT). If the gradient intensity of the pixel was higher than UT, the pixel was accepted as forming an edge and was set to a white pixel in a binary image. Otherwise, if the gradient intensity of the pixel was lower than LT, the pixel was rejected, classified as a non-edge pixel and set to a black pixel on the binary image. If the pixel intensity was between the two thresholds (UT and LT), the pixel was classified as an edge only if it was connected to an existing edge pixel. The filter returned binary images in which the white pixels identified as edges were used as an approximation for the real edges of the original images. We defined the sharpness score as the sum of white pixels in the binary image.

2.5.3. Cortico-medullary difference

To evaluate the difference in signal intensity (SI) between the cortex and medulla, ROIs were drawn in a minimum of 3 slices of the anatomic GRE of the healthy volunteers and copied onto the diffusion-weighted images. On each b-value image, regions of interest were placed in the cortex and medulla of the upper, mid and lower poles. In case of severe geometric distortion, some of the ROIs were manually corrected. For each b-value, the cortex and medulla were analyzed separately, and the mean SI was calculated as the mean of all voxels included in ROIs.

2.5.4. ADC

The apparent diffusion coefficient (ADC) was measured on quantitative ADC maps generated using a monoexponential model on a voxel-by-voxel basis according to the following formula:

$$\mathrm{ADC} = \frac{1}{b}\log\left(\frac{S_{voxel(b=0)}}{S_{voxel}}\right) \quad (1)$$

The ADC values were then averaged in each cortical and medullary ROI as defined above and expressed as mean ± standard deviation.

2.5.5. Qualitative assessment

Finally, all anonymized DW images were presented to a radiologist specialized in uro-radiology (20 years experience) in a blinded and random order for a qualitative visual assessment with regard to the ability to detect small structures, geometric distortions due to susceptibility, cortico-medullary difference and image blurring. A scale ranging from 0 (unacceptable image quality severely deteriorated by artifact) to 4 (artifact-free image without geometric distortions and with high anatomic details) was used to evaluate the overall preference of the radiologist.

2.5.6. Patient images

To further demonstrate the feasibility of the RESOLVE sequence in a clinical setting, the same acquisition protocol was repeated on 10 CKD patients. Selected examples were provided as an illustration of the image quality obtained in a clinical exam. Distortions, sharpness of images and ADC were analyzed as for healthy volunteers. However, the patients' ADC was compared to the values obtained in volunteers and not correlated with their own clinical data, as this will be the subject of an ongoing clinical study.

2.5.7. Statistical method

Statistical analysis, except for the qualitative assessment, was carried out using one-way analysis of variance (ANOVA) with post-hoc Bonferroni (SPSS software, version 21.0; Chicago, Illinois, USA). The qualitative assessment was analysis using non-parametric Wilcoxon signed-rank test. A value of $p < 0.05$ was taken as statistically significant.

3. Results

3.1. Phantom studies

3.1.1. Geometric distortions

The level of geometric distortions in the phantom is shown in Fig. 1a. The strongest deformation of the phantom borders was observed with the reference EPI, followed by the HR-EPI as quantified by the deviation from the corner of the phantom on the undistorted GRE reference image. The RESOLVE images were characterized by the smallest geometrical deformation among all the sequences. The maximum distance in the phase-encoding direction between the phantom edges of the GRE image and the reference EPI, HR-EPI, RESOLVE images was 1.34 cm, 0.95 cm and 0.47 cm respectively. The geometric distortion was therefore less pronounced for RESOLVE (35% of the reference EPI geometric distortion) than for the HR-EPI (71% of the reference EPI geometric distortion).

3.2. In vivo study

3.2.1. Geometric distortions

Representative in-vivo DW images performed in healthy volunteers, and patients are provided in Fig. 1 (b and c), 2 and 3. Reference EPI images suffered from severe deformations of the kidney border, especially in proximity of the air filled colon. Local deformation of the contours can easily be seen in reference and HR-EPI images. HR-EPI images were less distorted compared to the reference EPI. However, some significant geometric distortions were still visible with this sequence. In all case, the RESOLVE strategy drastically reduced the geometric distortion and the associated heterogeneity of the SI even in regions in close contact to air filled bowel. The whole parenchyma, especially the lower pole of the cortex, was much better delineated on the RESOLVE images than on the two ss-EPI images. As well as these geometric distortions Fig. 3 also illustrates the b_0 images of reference EPI, HR-EPI and RESOLVE MR images of a renal allograft in direct contact with the bladder and a renal allograft with visible scar following recurrent episodes of pyelonephritis (eGFR = 57 ml/min/1.73m^2) which is more distinct with RESOLVE. Stronger geometric distortions and blurring are clearly visible on both ss-EPI (reference and HR) images compared to RESOLVE images. (See Fig. 2.)

3.2.2. Blurring

The improvement of images resulting in reduced EPI blurring by application of the RESOLVE strategy could also be quantified with the 'Canny' filter. The RESOLVE strategy significantly improved the quantitative sharpness score (corresponding to the number of white "edge" pixels, as illustrated in Fig. 4 of RESOLVE images compared to HR-EPI. On average the sharpness score was 348 ± 150 pixels for RESOLVE, against 263 ± 133 pixels for HR-EPI ($p = 0.007$) and taking the average of the individual improvements, a 56% ± 86% higher score was obtained after applying the hysteresis threshold of the 'Canny' filter. The bar graph showing the sharpness value of all kidney images (healthy volunteers and patients) is shown in Fig. 5.

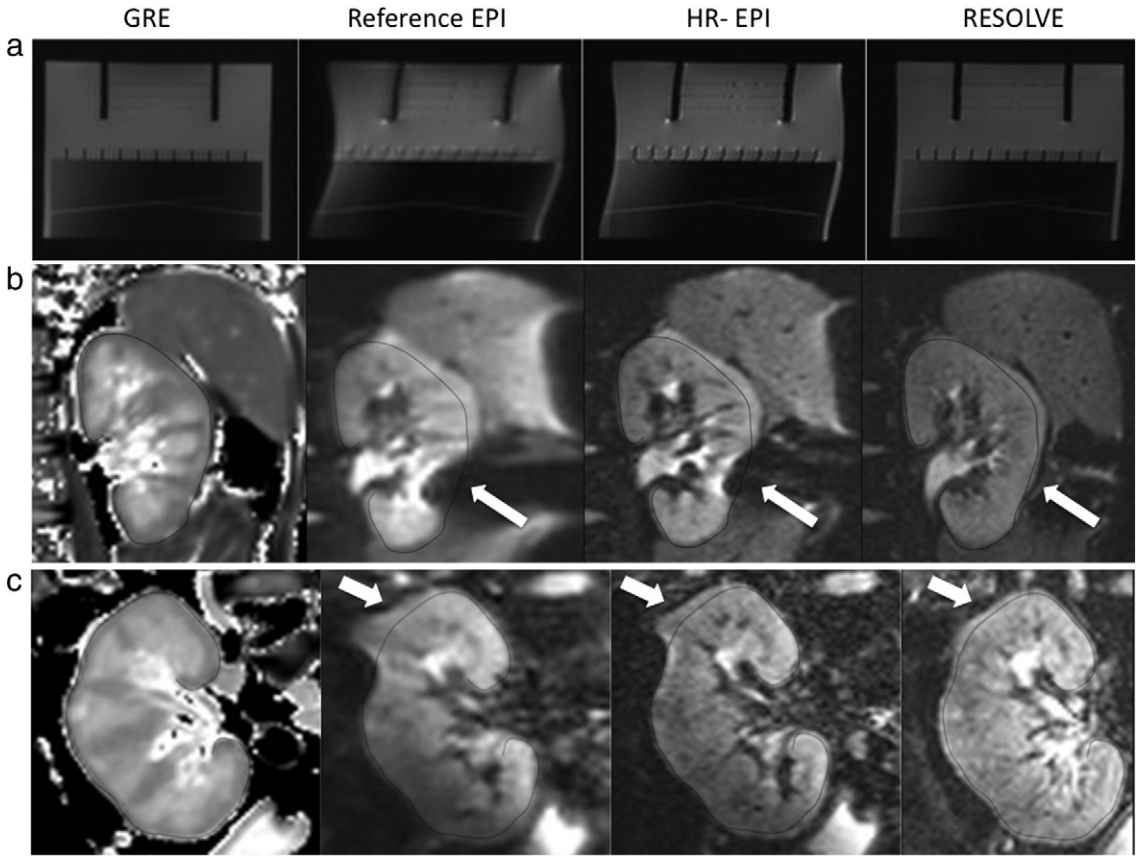

Fig. 1. Geometric distortions. a: Images of a phantom acquired with the same sequences (reference EPI, HR-EPI, RESOLVE and GRE) and imaging parameters as in volunteers and patients' experiments. GRE images used as reference. Strong geometric distortions and blurring are clearly more visible on single-shot EPI (reference and HR) compared to RESOLVE. b: b_0 images of left kidney of a healthy 24 year-old male. c: b_0 images of allograft in a 59 year-old male patient with 20% of fibrosis on biopsy. Contours of the GRE of b and c, considered to represent the true renal contours were drawn manually around kidney (dark line) and copied to the 3 diffusion MR images to show the reduced distortion of the RESOLVE images by comparison with the other sequences. White arrows point to areas of geometric distortions that are drastically reduced in the RESOLVE images.

In 38/43 cases the sharpness value was higher in RESOLVE compared to HR-EPI (with an average improvement of a 65% ± 89% higher score), indicating a better definition of the renal edges acquired with the RESOLVE sequence. In the 5 volunteers where the sharpness score was higher for HR-EPI than RESOLVE, the difference was always very small (9% ± 9%).

3.2.3. Cortico-medullary difference

The difference in mean SI between the cortex and medulla was improved on the RESOLVE images of the volunteers. This was significant (on b_0 images ($p = 0.0025$) and $b = 300$ seconds/mm^2 images ($p = 0.019$) with a ratio of mean SI between the cortex and medulla of 1.3 (b_0) and 1.2 (b_{300}). On the HR-EPI, only the b_0 images showed a difference ($p = 0.0028$) for HR-EPI with a ratio of mean SI between the cortex and medulla of 1.1 (b_0). No significant cortico-medullary difference was observed in reference EPI, even on the b_0 images.

3.2.4. ADC

Separate ADC values for the cortex and medulla were calculated. Both HR-EPI and RESOLVE, but not reference EPI, had significant ADC difference between the cortex and medulla of healthy volunteers, as shown in Fig. 6. In healthy volunteers, the mean ADC values (in 10^{-6} mm^2/s) was for reference EPI 2141 ± 244 in the cortex and 2092 ± 173 in the medulla ($p = 0.51$), for HR-EPI 2008 ± 254 in the cortex and 1817 ± 224 in the medulla ($p < 0.001$) and for RESOLVE 1994 ± 246 in the cortex and 1762 ± 238 for RESOLVE in the medulla ($p < 0.001$). The ADC difference between the cortex and medulla was not statistically different comparing RESOLVE and HR-EPI ($p = 0.63$ for cortex, $p = 0.19$ for medulla) and RESOLVE and reference EPI ($p = 0.80$ for cortex, $p = 0.09$ for medulla). In patients, the mean ADC values (in 10^{-6} mm^2/s) measured from the RESOLVE sequence were not different between the cortex (1755 ± 145) and the medulla (1799 ± 163, $p = 0.49$). Significant statistical ADC difference between healthy volunteers and patients was found in the cortex ($p < 0.001$) but not in the medulla ($p = 0.90$).

3.2.5. Qualitative assessment

RESOLVE showed the preferred image quality for all the parameters studied. The mean scores across 20 healthy volunteers for RESOLVE, HR-EPI and reference EPI in terms of geometric distortions, sharpness, and the cortico-medullary difference are shown in Fig. 7. Qualitatively, there was less geometric distortion of the kidney edges in every case (20/20) with RESOLVE vs. HR-EPI ($p = 0.02$) and vs. reference EPI ($p < 10^{-8}$). RESOLVE was considered sharper than reference EPI in all the cases ($p < 10^{-8}$) and, in 12/20 cases when comparing RESOLVE and HR-EPI (with an overall significant difference, $p = 0.001$). RESOLVE was considered just as sharp as HR-EPI in 7/20 cases. For the cortico-medullary contrast, RESOLVE performed better than HR-EPI in 7/20 cases ($p = 0.342$). Bringing together all qualitative parameters, the RESOLVE score was significantly higher than single-shot EPI score ($p < 0.05$).

4. Discussion

Our goal was to study the potential of readout-segmented echo-planar imaging with a fivefold segmented k-space acquisition for renal DWI. An improved image quality from the RESOLVE sequence

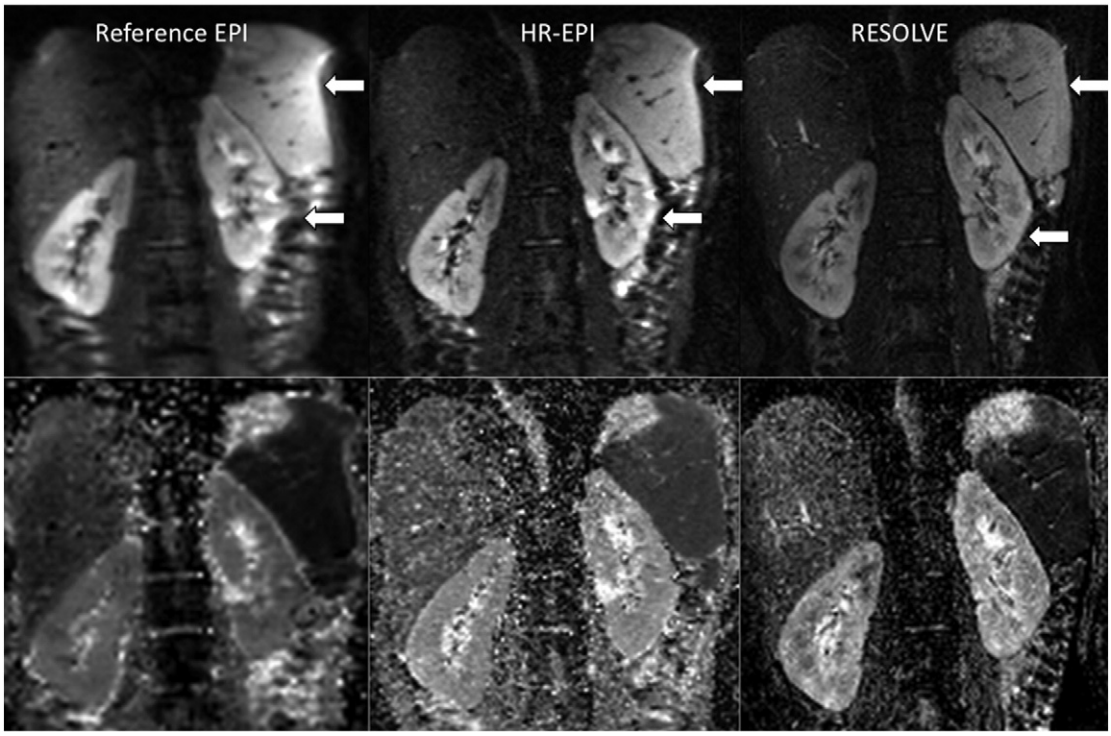

Fig. 2. Comparison of in vivo sequences in healthy volunteers. Coronal MR images of the kidneys in a 26-year-old female. Upper row: b_0 images of reference EPI, HR-EPI and RESOLVE. White arrows point to areas of geometric distortions and high signal intensity artifact at the bowel interface. Stronger geometric distortions and blurring are clearly visible on both single-shot SE-EPI (reference and HR) images compared to RESOLVE images. Furthermore, the difference between the cortex and medulla is sharper and better delineated on the RESOLVE images. Lower row shows the respective 4 b-value ADC maps with improved border definition on the RESOLVE image.

over ss-EPI sequences was observed in both healthy volunteers and CKD patients. The respiratory-gated RESOLVE significantly reduced diffusion artifacts and the other hurdles encountered with the use of ss-EPI. Whereas such improvements have already been demonstrated in the brain and breast [8–10,19–21], this is the first report of the use of RESOLVE in the abdominal cavity, which is strongly influenced by susceptibility artifacts resulting from the air/tissue interface in the bowel. In our study, we were able to show an almost complete absence of deformations of the kidney border at proximity of the bowel with the RESOLVE sequence by comparison of the ss-EPI sequence. A

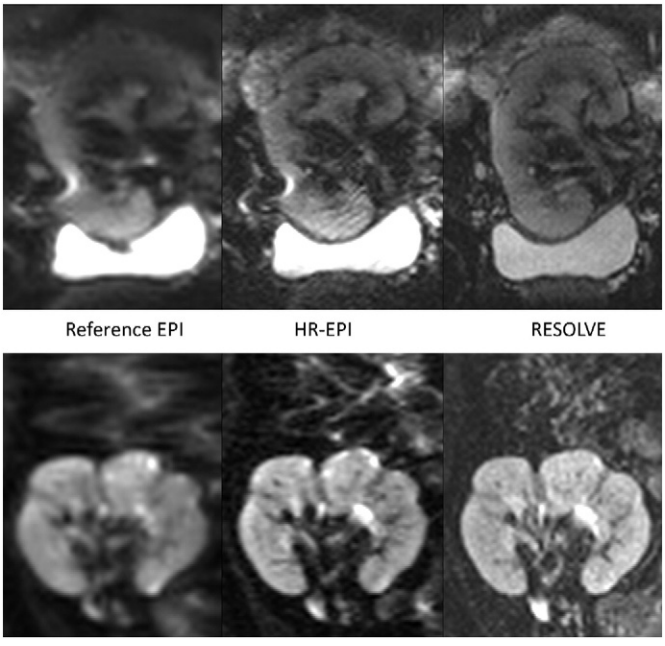

Fig. 3. Selective examples of the improvement of RESOLVE in two transplant patients. Coronal b_0 images of reference EPI, HR-EPI and RESOLVE MR images of a renal allograft in direct contact with the bladder in a 46-year-old male (upper row) and a renal allograft in 43-year-old female with visible scar following recurrent episodes of pyelonephritis (eGFR = 57 ml/min/1.73m^2). Stronger geometric distortions and blurring are clearly visible on both single-shot SE-EPI (reference and HR) images compared to RESOLVE images. Note also the improved visualization of the scars by the RESOLVE sequence in the lower row.

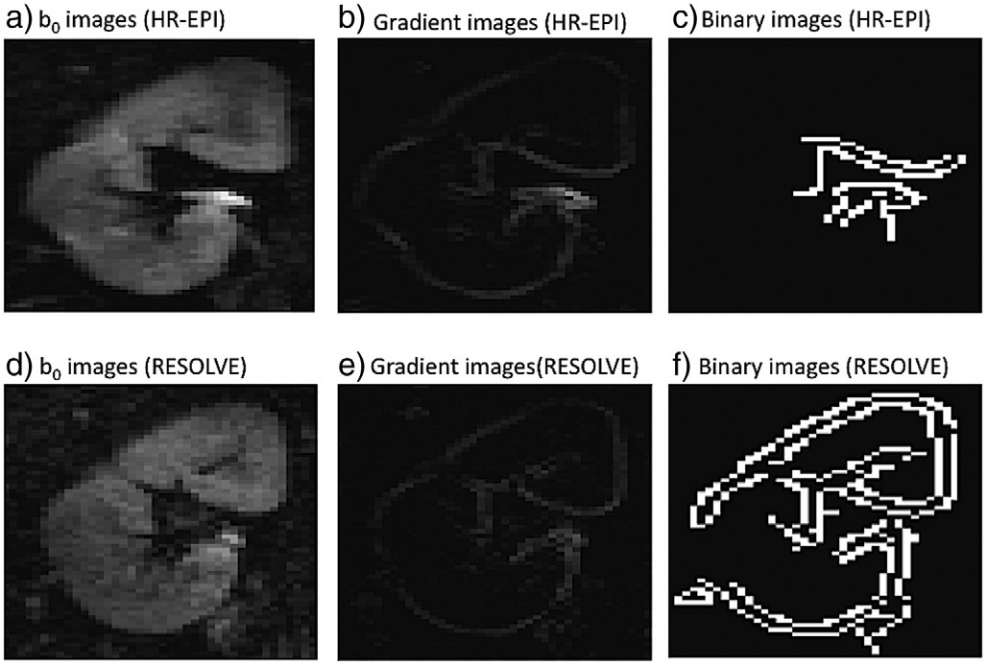

Fig. 4. Sharpness evaluation. The first column (a) and (d) shows the b_0 images of a healthy kidney using HR-EPI and RESOLVE sequences. (b) and (e) show the gradient images associated to the images (a) and (d). The kidney was better delineated with the RESOLVE strategy, as shown in the gradient images. On these images, a 'Canny' filter with a threshold of 0.4 was applied to evaluate the quality of the edges. The filter returned binary images (c) and (f) representative of the total number of "edge pixels" (white pixels) remaining after the application of the 'Canny' filter. The quantitative sharpness score was calculated as the number of white pixels (identifying an edge location). Analyzed regions were selected close around the kidney to avoid artifactual pixels from other organs. The sharpness scores calculated with the binary images were respectively 109 and 421 white pixels for HR-EPI and RESOLVE.

noteworthy achievement of our work was the high spatial resolution obtained with the RESOLVE sequence that outperformed previous published results at 3 T [22,23]. To compare RESOLVE with ss-EPI with the same spatial resolution, a standard ss-EPI (reference EPI) was set-up with optimized parameters (HR-EPI). Although some significant improvement was obtained with the shorter EPI echo-train length than the reference EPI as a result of the increased bandwidth and acceleration factor, HR-EPI was still less efficient at reducing the susceptibility artifacts than RESOLVE. This could be easily explained by the reduced effective echo-train resulting for the segmented acquisition.

Diffusion measurements are sensitive to differences in hardware (scanner performance) and acquisition parameters such as signal-to-noise and acquisition resolution. Additionally, positioning, alignment, warping, analysis software (segmentation and resectioning), data processing strategies (fit routine), and the absence of consensus in the b-values choice all play a role in the variability of ADC

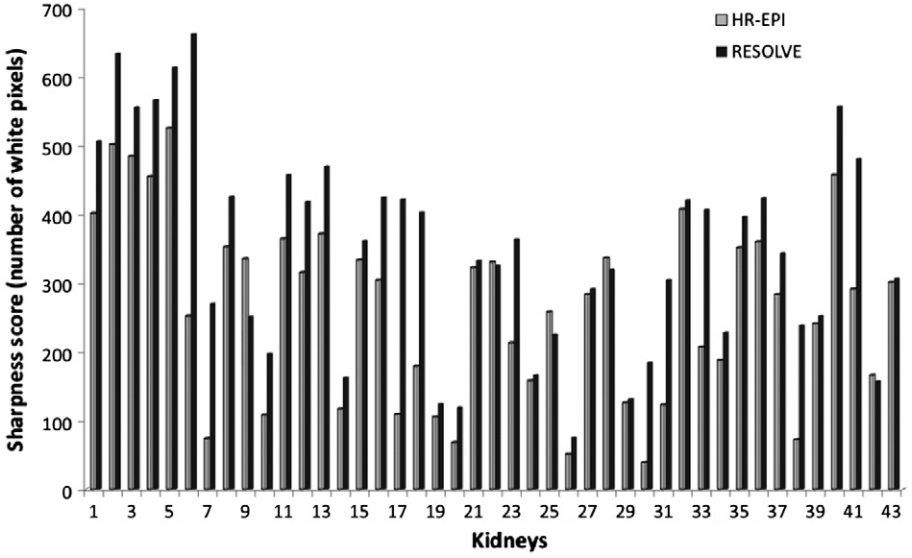

Fig. 5. Sharpness results of all kidneys: healthy and allograft. Bar graph showing the sharpness scores for each individual kidney ($n = 43$) calculated as the sum of white pixels remaining after the use of the 'Canny filter'. The hysteresis thresholding for the 'Canny filter' was 0.16 and 0.4. In 38/43 kidneys, the sharpness score was higher in RESOLVE compared to HR-EPI (on average 56% higher, $p = 0.007$ between the two sequences) demonstrating the improved sharpness of the RESOLVE images.

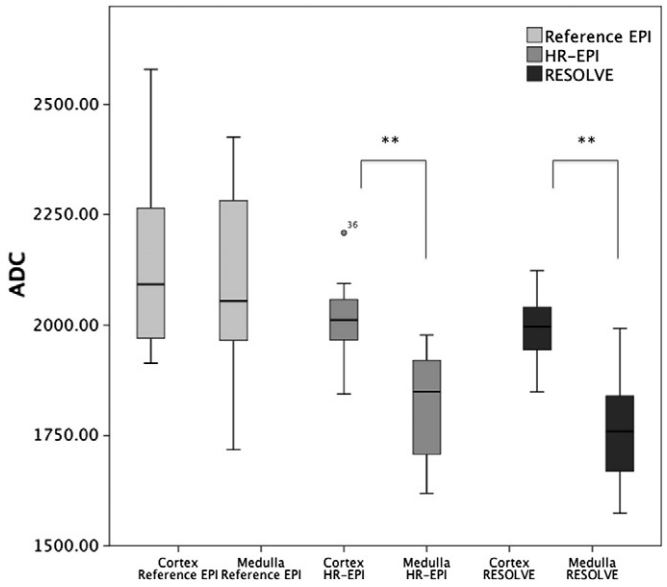

Fig. 6. ADC in healthy volunteers. Box plot illustrating the difference in mean ADC (10^{-6} mm^2/s) between the cortex and medulla with the 3 sequences: reference EPI, HR-EPI and RESOLVE. Data were obtained in both kidneys in 20 volunteers. A significant difference in ADC with $p < 0.001$ (**) is revealed between the cortex and medulla for RESOLVE and HR-EPI but not for reference EPI.

measurements especially for the cortico-medullary ADC difference [24,25]. In the present study, optimized protocol and hardware on a 3 T MR system allowed observation of the difference in ADC between the cortex and the medulla in healthy volunteers. This difference in ADC between the cortex and medulla was in agreement with recent studies on healthy volunteers [26,27]. In transplanted kidneys, the ADC was almost identical in the cortex and the medulla. The lack of a difference between these tissues could be explained by the denervation of the transplanted kidneys as well as the effects of immunosuppressive drugs [14]. An individual analysis of cortico-medullary ADC differentiation was not performed for each patient. Such an analysis would be worthwhile in future work, but is beyond the scope of the current study aiming to compare the image quality of the RESOLVE and ss-EPI protocols. However, we demonstrated that RESOLVE could really be applicable in clinical exams and enhanced significantly the image quality of patients by reducing the blurring and improving the robustness against distortions-related susceptibility artifacts. These results justified further study to evaluate the benefit of RESOLVE in patients.

In the present study, we introduced a new method to quantify and compare the sharpness between MR images based on the "Canny" edge detection algorithm. Such assessment was not performed in the previous published studies comparing RESOLVE and ss-EPI. We highlighted the significant higher sharpness of RESOLVE compared to HR-EPI, which has a similar nominal spatial resolution. Derivation methods developed to detect local intensity variation have been widely used in image processing for edge detection [28]. In cephalometric analysis, an algorithm based on the 'Canny' filter has been developed for automatic localization of craniofacial structures [29]. As such, the "Canny" method is often used in image processing, but not specifically for MR image analysis. Normally, MR studies have used sharpness based on profile through organ [30] or qualitative score [31]. The advantage of the 'Canny' filter is the quantification of the image sharpness based on the image edge detection method. In addition to a qualitative assessment of the MR images, we were, in this way, able to give a relevant quantitative score for the sharpness that is operator independent. As an additional advantage, our "Canny" edge methodology can easily be transferred to any other type of images comparison.

The main limitation of the RESOLVE sequence is the longer scan time. The increased acquisition time was directly proportional to the number of segments in the acquisition scheme. Although 5 times longer than a single-shot MR diffusion sequence acquisition, the scan time of the RESOLVE sequence (5'63" ± 1'53" measuring on healthy volunteers, against 1'07" ± 32" for Reference EPI and 1'11" ± 40" for HR-EPI) remained in the range of clinically acceptable MR sequences compared to, for example, respiratory gated coronary MR angiography [32]. In addition, the use of improved acceleration techniques such as compressed sensing could also provide a solution to reduce the acquisition time. Due to the relatively long imaging time of diffusion sequences, displacement of kidneys in the imaging

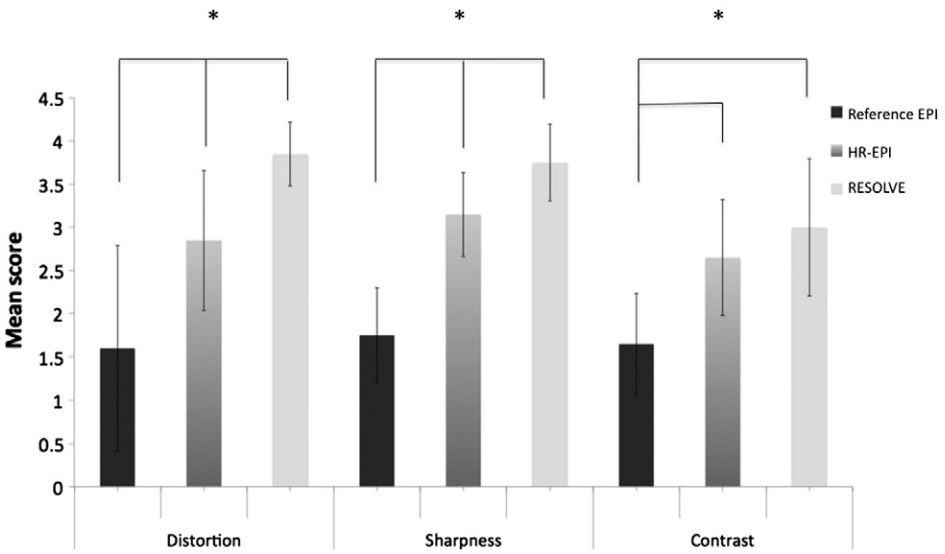

Fig. 7. Qualitative assessment in healthy volunteers. Bar graph showing mean scores of the overall imaging quality for visualizing both healthy kidneys separately. The following imaging parameters were under investigation: geometric distortion at susceptibility sites (e.g. proximity of air filled bowel), sharpness and the cortico-medullary contrast. The radiologist defined 0 as unacceptable image quality, severely deteriorated by artifact, and 4 as excellent for an artifact-free image without geometric distortions and with high anatomic details. Reference EPI, HR-EPI and RESOLVE were evaluated for 20 volunteers. $p < 0.05$ was taken as statistically significant.

plane during the scan is possible. Motion effects can be reduced by means of navigators or respiratory triggers as well as image registration techniques. Several registration techniques have sprung up over recent years to address this artifact in body applications subject to long acquisition time [33–35]. In liver diffusion, registration was applied to increase the robustness in multi-b-value acquisition [36]. A technique similar to the navigator-based RESOLVE reacquisition developed by Porter et al. [7] in head imaging for small motions could also have a potential for extension to renal diffusion.

As a limitation of our study, hydration status, which was not controlled, may explain some the variability between volunteers [37]. However, this should not compromise the comparison between sequences acquired during the same MR session and hydration status.

Although RESOLVE was superior in terms of image quality to the much shorter HR-EPI, we did not demonstrate in this study a clinical advantage of RESOLVE over HR-EPI in terms of patient's diagnosis or monitoring. This remains to be investigated by clinical studies. However, from our present result, RESOLVE can already be considered as the first choice of diffusion MR sequences in cases of severe susceptibility artifacts in the abdominal cavity.

5. Conclusions

In conclusion, despite a longer scan time, RESOLVE enhanced significantly the quality of renal diffusion-weighted images by reducing the image distortion and blurring and by improving the difference in SI and ADC between the renal cortex and medulla in healthy volunteers. The performance of the RESOLVE was also demonstrated in CKD patients with a disappearance of the cortico-medullary ADC difference. These improvements justify further clinical studies of the potential of RESOLVE for diffusion MRI.

Acknowledgements

This work was supported by grants from the Clinical Research Center of the Medicine Faculty of Geneva University and Geneva University Hospital and the Louis-Jeantet Foundation (CRC) and in part by the Centre for Biomedical Imaging (CIBM) of EPFL, University of Geneva and the University Hospitals of Geneva and Lausanne, as well as the Leenaards and Insuleman foundation.

References

[1] Squillaci E, Manenti G, Cova M, Di Roma M, Miano R, Palmieri G, et al. Correlation of diffusion-weighted MR imaging with cellularity of renal tumours. Anticancer Res 2004;24:4175–9.
[2] Thoeny HC, Zumstein D, Simon-Zoula S, Eisenberger U, De Keyzer F, Hofmann L, et al. Functional evaluation of transplanted kidneys with diffusion-weighted and BOLD MR imaging: initial experience. Radiology 2006;241:812–21.
[3] Faletti R, Cassinis MC, Fonio P, Grasso A, Battisti G, Bergamasco L, et al. Diffusion-weighted imaging and apparent diffusion coefficient values versus contrast-enhanced MR imaging in the identification and characterisation of acute pyelonephritis. Eur Radiol 2013;23:3501–8.
[4] Thoeny HC, Binser T, Roth B, Kessler TM, Vermathen P. Noninvasive assessment of acute ureteral obstruction with diffusion-weighted MR imaging: a prospective study. Radiology 2009;252:721–8.
[5] Yildirim E, Kirbas I, Teksam M, Karadeli E, Gullu H, Ozer I. Diffusion-weighted MR imaging of kidneys in renal artery stenosis. Eur J Radiol 2008;65:148–53.
[6] Le Bihan D, Poupon C, Amadon A, Lethimonnier F. Artifacts and pitfalls in diffusion MRI. J Magn Reson Imaging 2006;24:478–88.
[7] Porter DA, Heidemann RM. High resolution diffusion-weighted imaging using readout-segmented echo-planar imaging, parallel imaging and a two-dimensional navigator-based reacquisition. Magn Reson Med 2009;62:468–75.
[8] Holdsworth SJ, Yeom K, Skare S, Gentles AJ, Barnes PD, Bammer R. Clinical application of readout-segmented- echo-planar imaging for diffusion-weighted imaging in pediatric brain. AJNR Am J Neuroradiol 2011;32:1274–9.
[9] Bogner W, Pinker-Domenig K, Bickel H, Chmelik M, Weber M, Helbich TH, et al. Readout-segmented echo-planar imaging improves the diagnostic performance of diffusion-weighted MR breast examinations at 3.0 T. Radiology 2012;263:64–76.
[10] Iima M, Yamamoto A, Brion V, Okada T, Kanagaki M, Togashi K, et al. Reduced-distortion diffusion MRI of the craniovertebral junction. AJNR Am J Neuroradiol 2012;33:1321–5.
[11] Yeom KW, Holdsworth SJ, Van AT, Iv M, Skare S, Lober RM, et al. Comparison of readout-segmented echo-planar imaging (EPI) and single-shot EPI in clinical application of diffusion-weighted imaging of the pediatric brain. AJR Am J Roentgenol 2013;200:W437–43.
[12] Wisner DJ, Rogers N, Deshpande VS, Newitt DN, Laub GA, Porter DA, et al. High-resolution diffusion-weighted imaging for the separation of benign from malignant BI-RADS 4/5 lesions found on breast MRI at 3 T. J Magn Reson Imaging 2014;40:674–81.
[13] Taouli B, Sandberg A, Stemmer A, Parikh T, Wong S, Xu J, et al. Diffusion-weighted imaging of the liver: comparison of navigator triggered and breathhold acquisitions. J Magn Reson Imaging 2009;30:561–8.
[14] Thoeny HC, De Keyzer F. Diffusion-weighted MR imaging of native and transplanted kidneys. Radiology 2011;259:25–38.
[15] Padhani AR, Liu G, Koh DM, Chenevert TL, Thoeny HC, Takahara T, et al. Diffusion-weighted magnetic resonance imaging as a cancer biomarker: consensus and recommendations. Neoplasia 2009;11:102–25.
[16] Kyriazi S, Blackledge M, Collins DJ, Desouza NM. Optimising diffusion-weighted imaging in the abdomen and pelvis: comparison of image quality between monopolar and bipolar single-shot spin-echo echo-planar sequences. Eur Radiol 2010;20:2422–31.
[17] Qin Q. Point spread functions of the T2 decay in k-space trajectories with long echo train. Magn Reson Imaging 2012;30:1134–42.
[18] Canny J. A computational approach to edge detection. IEEE Trans Pattern Anal Mach Intell 1986;8:679–98.
[19] Robson MD, Anderson AW, Gore JC. Diffusion-weighted multiple shot echo planar imaging of humans without navigation. Magn Reson Med 1997;38:82–8.
[20] Brockstedt S, Moore JR, Thomsen C, Holtas S, Stahlberg F. High-resolution diffusion imaging using phase-corrected segmented echo-planar imaging. Magn Reson Imaging 2000;18:649–57.
[21] Holdsworth SJ, Skare S, Newbould RD, Guzmann R, Blevins NH, Bammer R. Readout-segmented EPI for rapid high resolution diffusion imaging at 3 T. Eur J Radiol 2008;65:36–46.
[22] Zhang JL, Sigmund EE, Rusinek H, Chandarana H, Storey P, Chen Q, et al. Optimization of b-value sampling for diffusion-weighted imaging of the kidney. Magn Reson Med 2012;67:89–97.
[23] Lanzman RS, Ljimani A, Pentang G, Zgoura P, Zenginli H, Kropil P, et al. Kidney transplant: functional assessment with diffusion-tensor MR imaging at 3 T. Radiology 2013;266:218–25.
[24] Zhang JL, Sigmund EE, Chandarana H, Rusinek H, Chen Q, Vivier PH, et al. Variability of renal apparent diffusion coefficients: limitations of the monoexponential model for diffusion quantification. Radiology 2010;254:783–92.
[25] Donati OF, Chong D, Nanz D, Boss A, Froehlich JM, Andres E, et al. Diffusion-weighted MR imaging of upper abdominal organs: field strength and intervendor variability of apparent diffusion coefficients. Radiology 2014;270:454–63.
[26] Wang WJ, Pui MH, Guo Y, Hu XS, Wang HJ, Yang D. MR diffusion tensor imaging of normal kidneys. J Magn Reson Imaging 2014;40:1099–102.
[27] Thoeny HC, De Keyzer F, Oyen RH, Peeters RR. Diffusion-weighted MR imaging of kidneys in healthy volunteers and patients with parenchymal diseases: initial experience. Radiology 2005;235:911–7.
[28] Caviedes J, Oberti F. A new sharpness metric based on local kurtosis, edge and energy information. Signal Process Image 2004;19:147–61.
[29] Mondal T, Jain A, Sardana HK. Automatic craniofacial structure detection on cephalometric images. IEEE Trans Image Process 2011;20:2606–14.
[30] Prieto C, Doneva M, Usman M, Henningsson M, Greil G, Schaeffter T, et al. Highly efficient respiratory motion compensated free-breathing coronary mra using golden-step Cartesian acquisition. J Magn Reson Imaging 2015;41:738–46.
[31] Chandarana H, Block KT, Winfeld MJ, Lala SV, Mazori D, Giuffrida E, et al. Free-breathing contrast-enhanced T1-weighted gradient-echo imaging with radial k-space sampling for paediatric abdominopelvic MRI. Eur Radiol 2014;24:320–6.
[32] Bi X, Deshpande V, Carr J, Li D. Coronary artery magnetic resonance angiography (MRA): a comparison between the whole-heart and volume-targeted methods using a T2-prepared SSFP sequence. J Cardiovasc Magn Reson 2006;8:703–7.
[33] Spiegel M, Hahn DA, Daum V, Wasza J, Hornegger J. Segmentation of kidneys using a new active shape model generation technique based on non-rigid image registration. Comput Med Imaging Graph 2009;33:29–39.
[34] Zollner FG, Sance R, Rogelj P, Ledesma-Carbayo MJ, Rorvik J, Santos A, et al. Assessment of 3D DCE-MRI of the kidneys using non-rigid image registration and segmentation of voxel time courses. Comput Med Imaging Graph 2009;33:171–81.
[35] Positano V, Bernardeschi I, Zampa V, Marinelli M, Landini L, Santarelli MF. Automatic 2D registration of renal perfusion image sequences by mutual information and adaptive prediction. MAGMA 2013;26:325–35.
[36] Mazaheri Y, Do RK, Shukla-Dave A, Deasy JO, Lu Y, Akin O. Motion correction of multi-b-value diffusion-weighted imaging in the liver. Acad Radiol 2012;19:1573–80.
[37] Sigmund EE, Vivier PH, Sui D, Lamparello NA, Tantillo K, Mikheev A, et al. Intravoxel incoherent motion and diffusion-tensor imaging in renal tissue under hydration and furosemide flow challenges. Radiology 2012;263:758–69.